This work has been accepted for publication in the 2022 IEEE International Conference on Communications Workshops (ICC Workshops), DOI:10.1109/ICCWorkshops53468.2022.9814622

Millimeter Wave vs. THz Energy Harvesting for Autonomous Reconfigurable Intelligent Surfaces

Konstantinos Ntontin* and Symeon Chatzinotas*

*SnT, SIGCOM, University of Luxembourg, Luxembourg,
e-mail: {kostantinos.ntontin, symeon.chatzinotas}@uni.lu

***Abstract*—The aim of this work is to examine the efficacy of wireless energy harvesting for autonomous reconfigurable intelligent surfaces that is performed either at millimeter wave or the lower THz bands. Towards this, we first consider an architecture in which a subset of unit cells is dedicated to energy harvesting and the rest to information transmission to a receiver through reflection. Subsequently, we compute the RIS energy consumption per frame according to the considered channel-estimation protocol. Based on it, we formulate an optimization problem that has as aim the maximization of the average rate under the constraint of meeting the RIS long-term energy consumption demands and provide its closed-form solution. Finally, numerical results are provided that target the performance comparison between the RIS-assisted links operating at the 28 GHz and 140 GHz bands. They reveal that the energy harvesting becomes more effective at the 140 GHz band, owing to the larger amount of unit cells that can be accommodated onto the same physical space.**

***Index Terms*—Reconfigurable intelligent surfaces, autonomous operation, wireless energy harvesting.**

I. Introduction

A. Background

To counteract the blockage bottleneck of high-frequency bands in forthcoming 6G networks, such as the millimeter-wave (mmWave) and terahertz (THz) bands, in a cost-efficient and low-energy consumption manner, the paradigm of reconfigurable intelligent surfaces (RISs) has been introduced the last years [1], [2]. The impedance of the unit cells (UCs) comprising such artificial structures can be properly tuned through semiconductor components, such as positive-intrinsic-negative (PIN) diodes, field-effect transistors (FETs), and radio-frequency microelectromechanical systems (RF-MEMS). This, in turn, allows the alteration of the amplitude and phase response to an impinging electromagnetic wave [3]. More specifically, the following different functionalities can be achieved: beam steering toward a desired angular direction or toward a desired point, beam splitting, and absorption. In terms of energy consumption, an amount of energy is consumed for their reconfigurability, but it is arguably significantly lower than the corresponding one of active nodes, since they do not require power amplifiers for their operation. This has led to the characterization of RISs as nearly passive structures [4]. This raises the question of whether RISs could operate autonomously by harvesting energy from wireless signals. Such a breakthrough has been suggested as a possibility for the so-called *integrated architecture* in which ultra low-power microcontrollers can be embedded onto an RIS structure for receiving wirelessly the reconfiguration commands and properly adjusting the impedance of the UCs [5–7]. In addition, few recent works have started incorporating the feature of autonomy [8–12].

B. Motivation, novelty, and contribution

As mentioned, RISs are more suitable to be deployed under mmWave or THz communication links since higher frequencies are more susceptible to blockage effects than their sub-6 GHz counterparts. On the other hand, such bands would at first seem less effective for power transmission to an RIS due to their increased free-space loss. However, such a rational does not take into account the higher gain of the antennas at the transmit end and also of the RIS since the number of radiating elements that can be accommodated onto the same physical space increases with frequency. Due to this, our goal in this work is to examine whether for increasing frequency of operation the supply of the energy needs of an autonomous RIS through energy harvesting of information signals becomes less effective. Based on this, our contribution is summarized as follows:

- We propose an energy harvesting protocol in which a subset of UCs is dedicated to energy harvesting and the rest for information transmission to an intended receiver through beamsteering. Furthermore, in contrast to previous works on autonomous RISs, the proposed protocol incorporates the channel estimation phase. Based on it, we prove that the RIS energy consumption that originates from channel estimation is substantially higher than the one required for adjusting the impedance of the UCs for information transmission.
- In contrast to previous works on autonomous RISs that consider subset allocation based on instantaneous channel estimates, in this work we consider a low-complexity offline scheme based on long-term statistics. Based on it, we provide the closed-form solution for the optimal number of UCs to be allocated to either energy harvesting or information transmission.
- Finally, as a case study for examining the efficacy of RIS wireless energy harvesting as the carrier frequency increases, we provide numerical results for the 28 GHz mmWave band and the 140 GHz lower THz band.

This work has been accepted for publication in the 2022 IEEE International Conference on Communications Workshops (ICC Workshops), DOI:10.1109/ICCWorkshops53468.2022.9814622

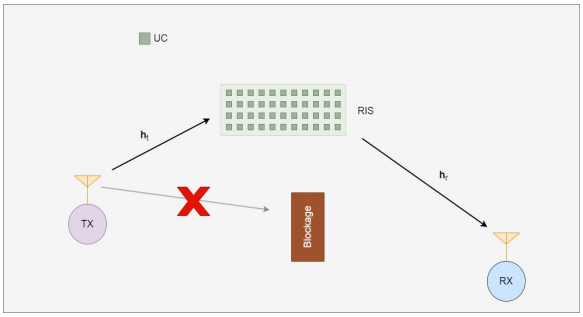

Fig. 1: Scenario.

The rest of this manuscript is structured as follows. In Section II, the system and channel models are presented together with the considered channel estimation protocol and the resulting RIS energy consumption per frame, according to the assumed power-consumption model. In Section III, we compute at first the harvested energy per transmission frame. Subsequently, we introduce the proposed energy harvesting architecture and, finally, we compute the end-to-end instantaneous SNR and achievable rate. In Section IV, the formulation of the problem of interest is presented together with its solution. Based on the analysis, numerical results are presented in Section V that examine the efficacy of wirelessly powering an RIS for increasing carrier frequency. Finally, the main takeaways of this work are summarized in Section VI.

II. System, Channel, and RIS Power-Consumption Models

A. System model

As illustrated in Fig. 1, we consider a scenario in which a directional transmitter (TX) of gain G_t communicates with a directional receiver (RX) of gain G_r through an RIS located in the far-field of both the TX and RX. The TX-RIS link, of distance d_t m, and RIS-RX link, of distance d_r m, constitute an alternative path to the direct TX-RX link that is assumed to be blocked. The RIS is a rectangular uniform planar array consisting of $M_s = M_x \times M_y$ UCs of size $d_x \times d_y$. M_x (M_y) and d_x (d_y) denote the number of UCs and their length in the x-axis (y-axis), respectively. In addition, we assume that the RIS is not equipped with an external power supply, but it relies on energy harvesting from the incoming power related to the information transmission of the TX. Through this harvested energy it can achieve autonomous operation. Finally, the transmission power from TX is equal to P_t.

B. Channel model

We assume a flat-fading channel model[1] where the complex envelope channel vectors of the TX-RIS and RIS-RX links denoted by $\mathbf{h}_t$ and $\mathbf{h}_r$, are given by

$$\mathbf{h}_{\mathrm{t}} = [h_{t_1} \quad \cdots \quad h_{t_{M_s}}]^T, \quad \mathbf{h}_{\mathrm{r}} = [h_{r_1} \quad \cdots \quad h_{r_{M_s}}]^T, \quad (1)$$

[1]Such an assumption would approximately hold for highly directional mmWave and THz transmissions that would result in small delay spreads and, hence, large coherence bandwidths.

where the UCs can be indexed arbitrarily. These vectors describe the joint effect of antenna gains, geometric pathloss, and multipath fading (i.e., the combination of small-scale and large-scale fading). In addition, we consider a block-fading model where the channel vectors are fixed within fixed-size time intervals, but change abruptly between intervals.

C. Channel-estimation protocol

Since an RIS does not include active RF chains and baseband units, intuitively only the cascaded TX-RIS-RX channel can be estimated either at the TX or RX. However, there are few works that consider extraction of knowledge of the separate $\mathbf{h}_{\mathrm{t}}$ and $\mathbf{h}_{\mathrm{r}}$ links [13–15]. The particular channel-estimation protocol to be followed has a direct impact on the power consumption of the RIS since in general, as the aforementioned works show, the effective channel estimation of the TX-RIS and RIS-RX links requires continuous reconfiguration of the RIS during the training period. Hence, the RIS needs reconfiguration not only when the quality of the links changes, but also for channel estimation. As a result, the higher the overhead for channel estimation is, the higher the RIS energy consumption is expected to be. To indicatively substantiate such power consumption requirements, in this work we consider the approach presented in [13] that is suitable for rank-deficient (sparse) TX-RIS and RIS-RX channels, as it is the case with mmWave and THz channels. By assuming that the preamble duration used for channel estimation is N_{pr} time slots and the pilot symbols sent by the TX are denoted by $x[t]$, $t = 1, 2, ..., N_{\mathrm{pr}}$, for the received samples at the RX during the preamble it holds that

$$y[t] = \mathbf{h}_{\mathrm{r}} (\mathbf{s}[t] \odot (\mathbf{h}_{\mathrm{t}} x[t])) + w[t], \quad t = 1, 2, ..., N_{\mathrm{pr}}, \quad (2)$$

where $w[t] \sim CN(0, \sigma^2)$ is the additive white Gaussian noise at the receiver and

$$\mathbf{s}[t] = \left[s_{1,t} e^{j\theta_{1,t}} \quad \cdots \quad s_{M_s,t} e^{j\theta_{M_s,t}} \right] \quad (3)$$

is the phase shift vector of the RIS with $s_{n,t} \in \{0, 1\}$. In addition, the RX has knowledge of both $x[t]$ and $\mathbf{s}[t]$ during the preamble phase. As described in [13], $s_{n,t}$ can be generated independently from a Bernoulli process with probability μ of taking the value 1 and the phases $\theta_{n,t}$ can take any value without affecting the effectiveness of the protocol. Hence, according to the law of large numbers, for a sufficiently large value of N_{pr} the number of 0's and 1's for each s_n in the preamble are equal to $(1-\mu) N_{\mathrm{pr}}$ and μN_{pr}, respectively. Normally, the recovery of the TX-RIS and RIS-RX links is more effective for low values of μ, as mentioned in [13], which means that the 'Off' states (0 value) of s_n would be notably higher than the 'On' states (1 value) during the preamble. Based on this, in the worst-case scenario the number of state changes for each s_n during the training period is equal to twice the number of its 'on' states, i.e. $2\mu N_{\mathrm{pr}}$. In addition, after the training period an additional reconfiguration of the RIS is needed where the impedance of the UCs is adjusted based on the channel estimates. Hence, the upper bound of

This work has been accepted for publication in the 2022 IEEE International Conference on Communications Workshops (ICC Workshops), DOI:10.1109/ICCWorkshops53468.2022.9814622

the total amount of reconfigurations for the M_s UCs, which we denote by $N_{\rm rec}^{\rm tot}$, is given by

$$N_{\rm rec}^{\rm tot} = N_{\rm rec}^{\rm CE} + N_{\rm rec}^{\rm IT} = M_s \left(2\mu N_{\rm pr} + 1\right), \tag{4}$$

where $N_{\rm rec}^{\rm CE}$ and $N_{\rm rec}^{\rm IT}$ denote the number of reconfigurations needed for the channel estimation (upper bound) and information transmission phases, respectively. They are given by

$$\begin{aligned} N_{\rm rec}^{\rm CE} &= 2M_s\mu N_{\rm pr} \\ N_{\rm rec}^{\rm IT} &= M_s. \end{aligned} \tag{5}$$

Hence, for typical values of $N_{\rm pr}$ required for reliable channel estimation[2] it holds that $N_{\rm rec}^{\rm CE} >> N_{\rm rec}^{\rm IT}$.

Moreover, in order to separate our work from imperfect channel estimation, which is out of scope, we assume that the preamble sequence length is sufficient so that the TX-RIS and RIS-RX links are perfectly estimated at the TX or RX.

Remark 1: We remark that with the proposed channel estimation protocol and methodology the amount of UC reconfigurations needed becomes independent of how fast the TX-RIS and RIS-RX links change, as long as they remain the same within one frame. Such an assumption of dedicated time slots for channel estimation is consistent with the operational principle of common communication protocols, such as Long Term Evolution [16].

D. RIS power-consumption model and total energy consumption per frame

1) RIS power-consumption model: To evaluate the total RIS power consumption per frame, we first need to identify the main RIS power-consuming modules, namely i) impedance-adjusting semiconductor components, ii) control network, and iii) rectifier. In this work, we consider the integrated architecture in which the control network consists of a network of communicating chips, one per UC. Both the impedance-adjusting semiconductor components and control chips exhibit a static and a dynamic power consumption. The latter power consumption is related to the charging and discharging of their internal capacitors during the reconfiguration phases.

Finally, for the RF-to-DC power conversion that is needed to power the electronic modules of the RIS, a passive rectifier circuit follows an RF combiner that combines the absorbed RF powers related to each UC.

2) RIS energy consumption per frame: Let us now evaluate the RIS energy consumption per frame, denoted by $E_{\rm tot}^{\rm fr}$. It holds that [17, Eq. (4.5)]

$$E_{\rm tot}^{\rm fr} = E_{\rm st}^{\rm fr} + E_{\rm dyn}^{\rm fr}, \tag{6}$$

where $E_{\rm st}^{\rm fr}$ and $E_{\rm dyn}^{\rm fr}$ denote the static and dynamic RIS energy consumption. The latter incorporates the consumption arising from both the control chips and impedance-adjusting semiconductor components.

Regarding $E_{\rm st}^{\rm fr}$, under the assumption of one control chip and one impedance-adjusting semiconductor component per UC, it is expected to scale linearly with the number of unit cells. Hence, if the total number of time slots per frame is $N_{\rm fr}$, their duration is $T_{\rm sl}$, and the static power consumption is $P_{\rm st}$, it holds

$$E_{\rm st}^{\rm fr} = M_s N_{\rm fr} T_{\rm sl} P_{\rm st}. \tag{7}$$

As far as $E_{\rm dyn}^{\rm fr}$ is concerned, based on (4) and denoting that the energy cost for a UC reconfiguration by $E_{\rm UC}$, the upper bound on $E_{\rm dyn}^{\rm fr}$ per frame is

$$E_{\rm dyn}^{\rm fr} = N_{\rm rec}^{\rm tot} E_{\rm UC} = E_{\rm rec}^{\rm CE} + E_{\rm rec}^{\rm IT} = M_s \left(2\mu N_{\rm pr} + 1\right) E_{\rm UC}, \tag{8}$$

where $E_{\rm rec}^{\rm CE} = 2M_s\lambda N_{\rm pr} E_{\rm UC}$ is the upper bound on the RIS energy consumption per frame related to channel estimation and $E_{\rm rec}^{\rm IT} = M_s E_{\rm UC}$ is the RIS energy consumption per frame related to reconfiguration for information transmission based on the channel estimates. Hence, based on the reasoning presented in Section II-C it holds $E_{\rm rec}^{\rm CE} >> E_{\rm rec}^{\rm IT}$, which means that the RIS energy consumption related to channel estimation is expected to be much larger than the required one for reconfiguration for information transmission. Based on (7) and (8), it holds

$$E_{\rm tot}^{\rm fr} = M_s \left(N_{\rm fr} T_{\rm sl} P_{\rm st} + \left(2\mu N_{\rm pr} + 1\right) E_{\rm UC}\right). \tag{9}$$

III. Harvested energy per frame and proposed architectures

A. Harvested energy per frame

Let us denote the set of the UCs used for energy harvesting (the same for each frame) by $\mathcal{A}_h$ and the set of all the UCs by $\mathcal{A}_s$, i.e.

$$\mathcal{A}_s = \{1, 2, ..., M_s\}. \tag{10}$$

Consequently, it holds that $\mathcal{A}_h \subseteq \mathcal{A}_s$. In addition, we denote the set of the UCs dedicated for reflection by $\mathcal{A}_r$. As a result, $\mathcal{A}_r$ is the orthogonal complement of $\mathcal{A}_r$, i.e. $\mathcal{A}_r = \mathcal{A}_h^C$. Finally, the number of UCs in $\mathcal{A}_h$ and $\mathcal{A}_r$ is denoted by M_h and M_r, respectively. Hence, $M_h + M_r = M_s$.

As far as the DC harvested power is concerned at a time slot of the $n_{\rm th}$ frame dedicated for energy harvesting, which we denote by $P_{\rm DC}\left(\mathcal{A}_h\right)$, it holds [18]

$$P_{\rm DC}\left(\mathcal{A}_h\right) = \frac{\frac{P_{\max}}{1+e^{-a\left(P_{\rm RF}\left(\mathcal{A}_h\right)-b\right)}} - \frac{P_{\max}}{1+e^{ab}}}{1 - \frac{1}{1+e^{ab}}}, \tag{11}$$

where $P_{\rm RF}\left(\mathcal{A}_h\right)$ is the harvested RF power that is inputted to the rectifier and $P_{\max}$ is a constant denoting the maximum harvested power when the harvesting circuit at the rectifier is saturated. In addition, a and b are circuit-specific parameters, which are related to the resistance, capacitance, and turn-on voltage of the diode used for rectification.

Regarding $P_{\rm RF}\left(\mathcal{A}_h\right)$, it is given by

$$P_{\rm RF}\left(\mathcal{A}_h\right) = \eta_{\rm RF} P_t \sum_{i \in \mathcal{A}_h} \left|h_{t_i}\right|^2, \tag{12}$$

[2] In [13] the authors show that $N_{\rm pr}$ should be in the order of hundreds of time slots to achieve sufficiently accurate channel estimation.

This work has been accepted for publication in the 2022 IEEE International Conference on Communications Workshops (ICC Workshops), DOI:10.1109/ICCWorkshops53468.2022.9814622

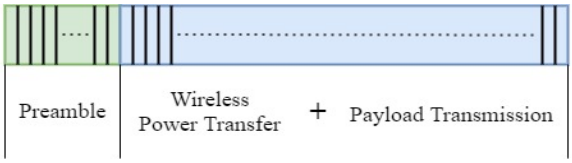

Fig. 2: Frame structure.

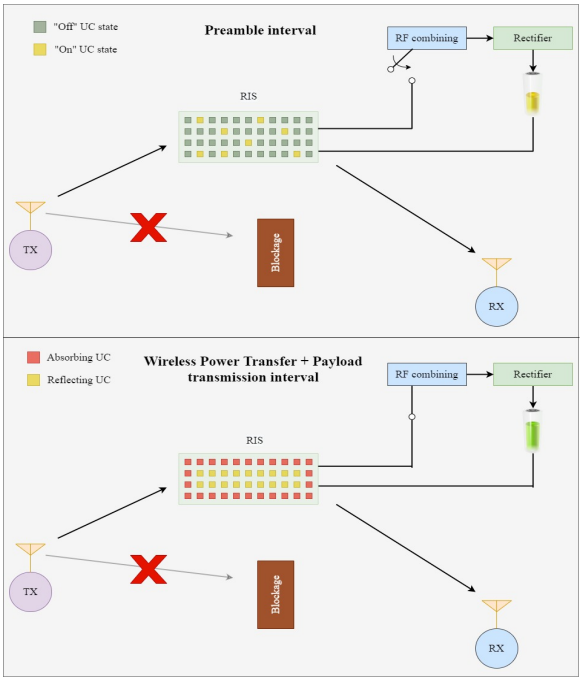

Fig. 3: RIS functionality during the preamble and payload transmission intervals.

where $\eta_{\mathrm{RF}} \in (0,1]$ denotes the efficiency of combining the individual harvested powers from each UC.

Finally, by denoting the number of time slots (the same for each frame) dedicated for energy harvesting by N_h and the amount of the respective harvested energy by E_h, it holds

$$E_h = P_{\mathrm{DC}}\left(\mathcal{A}_h\right) N_h T_{\mathrm{sl}}. \tag{13}$$

B. Architecture

The frame structure is depicted in Fig. 2. After the preamble transmission used for channel estimation, simultaneous wireless power transfer and information transmission is realized by dedicating a subset of UCs for energy harvesting through perfect absorption and the rest for information transmission by acting as perfect reflectors and focusing towards the RX. Illustratively, the functionality of the RIS for each of the 2 involved time intervals of a frame is depicted in Fig. 3.

In addition, it holds

$$N_{\mathrm{fr}} = N_{\mathrm{pr}} + N_{\mathrm{pl}}. \tag{14}$$

C. Instantaneous end-to-end SNR and rate

1) SNR: The instantaneous end-to-end SNR related to the information transmission, denoted by γ, can be obtained by following the standard approach as [19]

$$\gamma = \frac{P_t}{\sigma^2}\left(\sum_{k\in\mathcal{A}_r} |h_{t_k}|\,|h_{r_k}|\right)^2, \tag{15}$$

where $\sigma^2 = -174 + 10\log_{10}(W) + \mathcal{F}_{\mathrm{dB}}$ is the noise level at the receiver with W being the bandwidth and $\mathcal{F}_{\mathrm{dB}}$ the noise figure at the receiver in dB.

2) Rate: Based on (15), the instantaneous rate, denoted by R, is given by

$$R = \frac{N_{\mathrm{pl}}}{N_{\mathrm{fr}}} W \log_2\left(1 + \frac{P_t}{\sigma^2}\left(\sum_{k\in\mathcal{A}_r} |h_{t_k}|\,|h_{r_k}|\right)^2\right), \tag{16}$$

IV. Problem Formulation and Solution

Let us present Lemma 1 before proceeding with the problem formulation.

Lemma 1: Let us consider a sufficiently large number of frames, denoted by K. Then, for the total amount of energy harvested in the particular duration, which we denote by $E_{1\to K}$, it holds

$$E_{1\to K} = \sum_{n=1}^{K} E_h = \left(N_{\mathrm{fr}} - N_{\mathrm{pr}}\right) T_{\mathrm{sl}} \sum_{n=1}^{K} P_{\mathrm{DC}}\left(\mathcal{A}_h\right) \tag{17}$$

$$\cong \left(N_{\mathrm{fr}} - N_{\mathrm{pr}}\right) T_{\mathrm{sl}} K E\left\{P_{\mathrm{DC}}\left(\mathcal{A}_h\right)\right\}, \tag{18}$$

where $E\{\cdot\}$ denotes average value.

Proof: The proof of Lemma 1 follows by considering that $N_h = N_{\mathrm{fr}} - N_{\mathrm{pr}}$ and $\sum_{n=1}^{K} P_{\mathrm{DC}}\left(\mathcal{A}_h\right) \cong K E\{P_{\mathrm{DC}}\left(\mathcal{A}_h\right)\}$ due to the law of large numbers for sufficiently large K.

The problem formulation concerning the maximization of the average rate in the duration of the K frames is as follows:

Average rate maximization:

$$\begin{aligned} \underset{M_r}{\text{maximize}} \quad & E^{(K)}\left\{R\left(M_r\right)\right\} \\ \text{subject to} \quad & E_{1\to K} \geq K E_{\mathrm{tot}}^{\mathrm{fr}}, \end{aligned} \tag{19}$$

where $E^{(K)}\{\cdot\}$ denotes the average value for the K frame duration. It holds

$$\begin{aligned} E^{(K)}\left\{R\left(M_r\right)\right\} &\overset{(\alpha)}{\cong} E\left\{R\left(M_r\right)\right\} \\ &\overset{(b)}{=} \frac{N_{\mathrm{pl}}}{N_{\mathrm{fr}}} W \log_2(e) \int_0^{\infty} \frac{1 - F_{\gamma_{M_r}}(x)}{1+x} dx, \end{aligned} \tag{20}$$

where in (α) we use the law of large numbers for sufficiently large K and in (b) we use (16) and [20, Eq. (38)]. $F_{\gamma_{M_s}}(x)$ denotes the CDF of γ.

Based on (11), (12), and (16), (20) can be rewritten as

$$\begin{aligned} \underset{M_r}{\text{maximize}} \quad & \int_0^{\infty} \frac{1-F_{\gamma_{M_r}}(x)}{1+x} dx \\ \text{subject to} \quad & Q\left(M_h\right) \geq \left(1 - \frac{1}{1+e^{ab}}\right) \frac{E_{\mathrm{tot}}^{\mathrm{fr}}}{\left(N_{\mathrm{fr}} - N_{\mathrm{pr}}\right) T_{\mathrm{sl}}} + \frac{P_{\max}}{1+e^{ab}}, \end{aligned} \tag{21}$$

where

$$Q\left(M_h\right) = \int_0^{\infty} \frac{P_{\max}}{1 + e^{-a\left(\eta_{\mathrm{RF}} P_t x - b\right)}} f_{|h_{t_{M_h}}|}(x)\, dx. \tag{22}$$

This work has been accepted for publication in the 2022 IEEE International Conference on Communications Workshops (ICC Workshops), DOI:10.1109/ICCWorkshops53468.2022.9814622

$f_{|h_{t_{M_h}}|}(x)$ is the pdf of $\sum_{i=1}^{M_h}|h_{t_i}|^2$ and $F_{|h_{t_{M_r}}||h_{r_{M_r}}|}(x)$ is the CDF of $\left(\sum_{k=1}^{M_r}|h_{t_k}||h_{r_k}|\right)^2$.

Proposition 1: The solution of (21), denoted by M_r^*, is given by $M_r^* = M_s - M_h^*$, where

$$M_h^* = \left\lceil Q^{-1}\left(\left(1-\frac{1}{1+e^{ab}}\right)\frac{E_{\rm tot}^{\rm fr}}{(N_{\rm fr}-N_{\rm pr})T_{\rm sl}} + \frac{P_{\max}}{1+e^{ab}}\right)\right\rceil \tag{23}$$

and $M_r^* = M_s - M_h^*$.

Proof: The proof of Proposition 1 follows by considering that (21) is solved by the M_h value, denoted by M_h^*, that gives the equality in the constraint.

V. Numerical Results

The aim of this section is to leverage the analytical results of Section IV to examine the efficacy of wireless energy harvesting for an autonomous RIS at the 28 GHz and 140 GHz bands. Towards this, for a fair comparison we assume that the physical space occupied by the TX/RX antennas and the RIS is the same in both cases. For the TX and RX antennas we assume, without loss of generality, that consist of parabolic reflector antennas with diameters D_t and D_r, respectively. Hence, their maximum gains at the broadside, are given by

$$G_m = e_m\left(\frac{\pi D_m}{\lambda}\right)^2, \quad m \in \{t, r\}, \tag{24}$$

where λ is the wavelength and e_t, e_r the efficiencies of the TX and RX antennas, respectively. Furthermore, we consider that each UC is an electrically-small low-gain element with a gain pattern, with respect to the azimuth angle θ, expressed as

$$G_s(\theta) = 4\cos(\theta), \quad 0 \le \theta < \pi/2. \tag{25}$$

This model is supported by measurements [21].

As far as the channel model is concerned, without loss of generality we assume that it follows free-space propagation, which would approximately hold for highly directional transmissions expected at mmWave and THz bands. Hence, it holds

$$\begin{aligned}\mathbf{h}_{\rm t} &= \sqrt{\left(\frac{\lambda}{4\pi}\right)^2\frac{G_tG_s(\theta_{\rm inc})}{d_t^2}}\left[e^{j\frac{2\pi}{\lambda}d_{t_1}} \ \cdots \ e^{j\frac{2\pi}{\lambda}d_{t_{M_s}}}\right]\\ \mathbf{h}_{\rm r} &= \sqrt{\left(\frac{\lambda}{4\pi}\right)^2\frac{G_rG_s(\theta_{\rm dep})}{d_r^2}}\left[e^{j\frac{2\pi}{\lambda}d_{r_1}} \ \cdots \ e^{j\frac{2\pi}{\lambda}d_{r_{M_s}}}\right],\end{aligned} \tag{26}$$

where d_{t_k}, d_{r_k}, $k = 1, 2, ..., M_s$, are the distances between the TX and the center of the $k_{\rm th}$ UC and between the center of the $k_{\rm th}$ UC and the RX, respectively. Furthermore, $\theta_{\rm inc}$ and $\theta_{\rm dep}$ denote the incident angle on the RIS and departure angle from the RIS of the propagating wave, respectively.

Let us note that atmospheric absorption that becomes prominent in the THz spectrum has an approximately negligible effect for the lower THz bands, such as the 140 GHz band that we consider in this work [22]. This is the reason that we have not taken it into account.

We remark that based on (24) and (26) the higher free-space dissipation for smaller wavelengths is fully compensated by the increase of the TX antenna gain. Hence, in the comparison of the energy harvesting efficacy between the 28 GHz and 140 GHz bands, only the RIS part becomes relevant. For such a comparison, we consider the parameter values of Table I. The considered RIS size is 8 cm x 8 cm, which accommodates 15 and 75 UCs in each dimension for the 28 GHz and 140 GHz, respectively. In addition, we note that with the considered d_t of 21 m, the RIS in both cases of 28 GHz and 140 GHz is located in Fraunhofer region of the TX antenna. As far as the results are concerned, firstly in Fig. 4 we examine how $E\{R(M_r^*)\}$ varies with respect to $E_{\rm UC}$ for two values of $P_{\rm st}$. As we observe, not only a substantially higher average rate is achieved for the 140 GHz case, but also the range of $E_{\rm UC}$ values for which the RIS UCs are adequate to supply its energy needs is higher. Even if we take into account that in practical implementations circuits at 140 GHz would most likely exhibit a higher $P_{\rm st}$ than the 28 GHz band (due to more pronounced leakage current effects at higher frequencies), we still observe that for 140 GHz $E\{R(M_r^*)\}$ in the $P_{\rm st} = 1$ μW case is notably higher than the corresponding one of 28 GHz in the $P_{\rm st} = 0.2$ μW case for a large range of $E_{\rm UC}$. Finally, to further substantiate the benefits of a notably higher number UCs that are accommodated in the RIS in the 140 GHz case compared with its 28 GHz counterpart, in Fig. 5 we illustrate how the percentage of UCs dedicated to reflection varies with $E_{\rm UC}$. As we observe, not only this percentage is higher in the 140 GHz case, but the gap with respect to the 28 GHz case increases as the $E_{\rm UC}$ increases. In particular, we observe that for $E_{\rm UC} = 1$ pJ the gap is around 12%, whereas it is around 18% for $E_{\rm UC} = 10$ pJ.

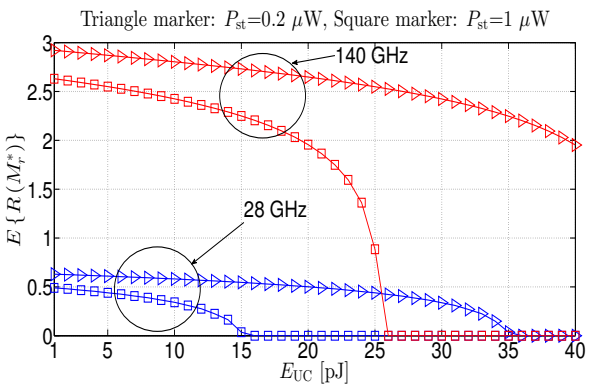

Fig. 4: $E\{R(M_r^*)\}$ vs. $E_{\rm UC}$.

VI. Conclusions

We have conducted this work to give an answer on whether wireless energy harvesting for supplying the energy needs of an autonomous RIS is more effective at a mmWave band or a lower THz band, in particular the 28 GHz and 140 GHz bands, respectively. Such bands find application in various scenarios that are related to future access networks or wireless backhauling. Towards this, we have first considered an architecture that allocates a subset of UCs to energy harvesting and the rest to information transmission. Subsequently, we have computed the RIS energy consumption per frame and formulated an

This work has been accepted for publication in the 2022 IEEE International Conference on Communications Workshops (ICC Workshops), DOI:10.1109/ICCWorkshops53468.2022.9814622

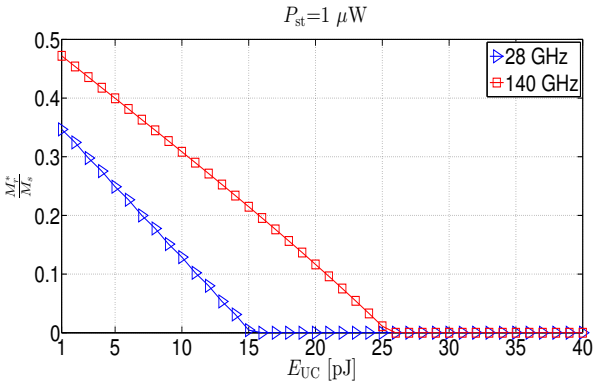

Fig. 5: $\frac{M_r^*}{M_s}$ vs. E_{UC}.

TABLE I: Parameter values used in the simulation.

Parameter	Value	Parameter	Value
d_x, d_y	$\lambda/2$	M_x, M_y	15 (28 GHz) 75 (140 GHz)
P_t	1 W	W	125 MHz (28 GHz) 375 MHz (140 GHz)
D_t, D_r	15 cm	$\mathcal{F}_{\text{dB}}$	10 dB
d_t	21 m	d_r	100 m
N_{fr}	10^4	N_{pr}	10^3
θ_{inc}	45°	θ_{dep}	60°
η_{RF}	0.5	a	120
b	10^{-3}	$P_{\max}$	20 mW
μ	0.2 μW	T_{sl}	1 μs
e_t	0.7	e_r	0.7

optimization problem that targets the maximization of the average rate subject to meeting the RIS long-term energy consumption demands and provided its closed-form solution. They reveal that energy harvesting is more effective at the 140 GHz band, which is attributed to the larger amount of UCs that can be accommodated onto the same physical space. The most important outcomes are that: i) operating at 140 GHz band allows a higher range of RIS energy consumption demands to be supplied by wireless energy harvesting and ii) a higher percentage of UCs is dedicated to reflection in the 140 GHz case and the gap with its 28 GHz counterpart increases as the RIS energy consumption demands increase as well.

ACKNOWLEDGEMENTS

This work has received funding from the Luxembourg National Research Fund (FNR) as part of the CORE programme under project RISOTTI C20/IS/14773976.

REFERENCES

[1] M. Di Renzo *et al.*, "Smart Radio Environments Empowered by Reconfigurable Intelligent Surfaces: How It Works, State of Research, and The Road Ahead," *IEEE J. Sel. Areas Commun.*, vol. 38, no. 11, pp. 2450–2525, Nov. 2020.

[2] E. Björnson, Ö. Özdogan, and E. G. Larsson, "Reconfigurable Intelligent Surfaces: Three Myths and Two Critical Questions," *EEE Commun. Mag*, vol. 58, no. 12, pp. 90–96, Dec. 2020.

[3] O. Tsilipakos *et al.*, "Toward intelligent metasurfaces: The progress from globally tunable metasurfaces to software-defined metasurfaces with an embedded network of controllers," *Advanced Optical Materials*, no. 2000783, July 2020.

[4] X. Yuan, Y.-J. A. Zhang, Y. Shi, W. Yan, and H. Liu, "Reconfigurable-Intelligent-Surface Empowered Wireless Communications: Challenges and Opportunities," *IEEE Wirel Commun.*, vol. 28, no. 2, pp. 136–143, April 2021.

[5] S. Abadal, T. Cui, T. Low, and J. Georgiou, "Programmable Metamaterials for Software-Defined Electromagnetic Control: Circuits, Systems, and Architectures," *IEEE J. Emerg. Sel. Topics Power Electron.*, vol. 10, no. 1, pp. 6–19, March 2020.

[6] A. C. Tasolamprou *et al.*, "Exploration of Intercell Wireless Millimeter-Wave Communication in the Landscape of Intelligent Metasurfaces," *IEEE Access*, vol. 7, pp. 122 931–122 948, Aug. 2019.

[7] C. Liaskos, S. Nie, A. Tsioliaridou, A. Pitsillides, S. Ioannidis, and I. Akyildiz, "Realizing Wireless Communication Through Software-Defined HyperSurface Environments," in *2018 IEEE 19th International Symposium on "A World of Wireless, Mobile and Multimedia Networks" (WoWMoM)*, 2018.

[8] Y. Zou, S. Gong, J. Xu, W. Cheng, D. T. Hoang, and D. Niyato, "Wireless Powered Intelligent Reflecting Surfaces for Enhancing Wireless Communications," *IEEE Trans. Veh. Techn.*, vol. 69, no. 10, pp. 12 369–12 373, Oct. 2020.

[9] Z. Chu, P. Xiao, D. Mi, W. Hao, M. Khalily, and L.-L. Yang, "A Novel Transmission Policy for Intelligent Reflecting Surface Assisted Wireless Powered Sensor Networks," *IEEE Journal of Selected Topics in Signal Processing*, vol. 15, no. 5, pp. 1143–1158, Aug. 2021.

[10] S. Hu, Z. Wei, Y. Cai, C. Liu, D. W. K. Ng, and J. Yuan, "Robust and Secure Sum-Rate Maximization for Multiuser MISO Downlink Systems with Self-sustainable IRS," *IEEE Trans. on Commun.*, vol. to appear, 2021.

[11] Y. Pan, K. Wang, C. Pan, H. Zhu, and J. Wang, "Self-Sustainable Reconfigurable Intelligent Surface Aided Simultaneous Terahertz Information and Power Transfer (STIPT)." [Online]. Available: https://arxiv.org/abs/2102.04053

[12] B. Lyu, P. Ramezani, D. T. Hoang, S. Gong, Z. Yang, and A. Jamalipour, "Optimized Energy and Information Relaying in Self-Sustainable IRS-Empowered WPCN," *IEEE Trans. Commun.*, vol. 69, no. 1, pp. 619–633, Jan. 2021.

[13] Z.-Q. He and X. Yuan, "Cascaded Channel Estimation for Large Intelligent Metasurface Assisted Massive MIMO," *IEEE Wirel. Commun. Lett.*, vol. 9, no. 2, Feb. 2020.

[14] C. Hu, L. Dai, S. Han, and X. Wang, "Two-Timescale Channel Estimation for Reconfigurable Intelligent Surface Aided Wireless Communications," *IEEE Trans. Commun.*, vol. to appear, 2021.

[15] G. T. de Araújo, A. L. F. de Almeida, and R. Boyer, "Channel Estimation for Intelligent Reflecting Surface Assisted MIMO Systems: A Tensor Modeling Approach," *IEEE Journal of Sel. Topics in Signal Proc.*, vol. 15, no. 3, pp. 789–802, 2021.

[16] C. Johnson, *Long Term Evolution IN BULLETS*. Northampton, England: Johnson, 2012.

[17] "Report on the comparison between ideal HyperSurface (HSF)s and the manufactured prototypes," VISORSURF project, Tech. Rep., Dec. 2020. [Online]. Available: https://ec.europa.eu/research/participants/documents/downloadPublic?documentIds=080166e5d7993c7d&appId=PPGMS

[18] E. Boshkovska, D. W. K. Ng, N. Zlatanov, and R. Schober, "Practical Non-Linear Energy Harvesting Model and Resource Allocation for SWIPT Systems," *IEEE Commun. Lett.*, vol. 19, no. 12, pp. 2082–2085, Dec. 2015.

[19] K. Ntontin, A.-A. A. Boulogeorgos, D. G. Selimis, F. I. Lazarakis, A. Alexiou, and S. Chatzinotas, "Reconfigurable Intelligent Surface Optimal Placement in Millimeter-Wave Networks," *IEEE Open J. Commun. Soc.*, vol. 2, pp. 704–718, March 2021.

[20] L. Yang, K. Qaraqe, E. Serpedin, and M.-S. Alouini, "Performance Analysis of Amplify-and-Forward Two-Way Relaying with Co-Channel Interference and Channel Estimation Error," *IEEE Trans. Commun.*, vol. 61, no. 6, pp. 2221–2231, June 2013.

[21] W. Tang, X. Chen, M. Z. Chen, J. Y. Dai, Y. Han, M. D. Renzo, S. Jin, Q. Cheng, and T. J. Cui, "Path Loss Modeling and Measurements for Reconfigurable Intelligent Surfaces in the Millimeter-Wave Frequency Band," *arXiv:1906.09490*.

[22] I. F. Akyildiz, J. M. Jornet, and C. Han, "Teranets: ultra-broadband communication networks in the terahertz band," *IEEE Wireless Commun.*, vol. 21, no. 4, pp. 130–135, Aug. 2014.